King Saud University

Arabian Journal of Chemistry

www.ksu.edu.sa
www.sciencedirect.com

ORIGINAL ARTICLE

Preparation, characterization and antioxidant activity of a novel polysaccharide-iron (III) from *Flammulina velutipes* scraps

Yingyun Peng, Han Jiang, Yufeng Wu, Jinlong Zhang, Yiyong Chen *

School of Biology and Food Engineering, Changshu Institute of Technology, China

Abstract In the present study, a novel polysaccharide from *Flammulina velutipes* scraps (FVSP) was extracted and purified from *Flammulina velutipes* scraps. FVSP was chemically chelated to synthesize FVSP-iron (III) complex. Based on single factor experiments, preparation process of FVSP-iron (III) was optimized by response surface methodology. The characterization and antioxidant activity of FVSP-iron (III) were investigated. The results showed that the optimal preparation process of FVSP-iron (III) was reaction temperature of 50 °C, reaction time of 4.7 h and the mass ratio of FVSP/sodium citrate - of 2:1. The relative molecular weight of FVSP-iron (III) was 36.25 kDa. FVSP-Iron (III) was composed of glucose, galactose, mannose and xylose in a molar ratio of 65.1:20.5:5.2:9.2.The results of UV–vis absorption spectrum, FI-IR spectrum and X-ray diffraction showed that both hydroxyl and carboxyl groups in FVSP participated in the coordination reaction and the iron core of FVSP-Iron(III) was a polymerized β-FeOOH structure. FVSP-iron (III) had better thermal stability and stronger antioxidant activities than FVSP. The results indicated that FVSP-iron (III) could be potentially used in food industry as a new food additive and iron supplement.

1. Introduction

As one of the essential trace elements for human growth and development, iron can participate in the synthesis of hemoglobin and enzymes, transport oxygen and nutrients, etc. (Danielson, 2004). Malnourished children and pregnant women are more likely to suffer from iron deficiency anemia (IDA), which is a common nutritional disease (Sarah et al., 2016; Denic and Agarwal, 2007). Iron supplementation is very important and necessary for the treatment and prevention of IDA (Wang et al., 2020). Therefore, it is necessary to develop a safe iron supplement with high availability and low side effects. Polysaccharide iron complex is a new type of biological and highly effective oral iron supplement which has been widely used in clinic (Zhang et al., 2012).

* Corresponding author at: School of Biology and Food Engineering, Changshu Institute of Technology, No. 99 Nansanhuan Road, Changshu 215500, Jiangsu Province, China.
E-mail address: greenpop6688@126.com (Y. Chen).

Many researches showed that polysaccharide iron complex had excellent application properties such as water solubility, high stability and good absorption in body (Wu et al., 2012). Galactomannan–iron(III) complexes synthesized from sesbania seed polysaccharides exhibited antioxidant activities and could be used as organic iron supplements to patients with iron deficiency (Huang et al., 2019). A new *Inonotus obliquus* polysaccharide-iron (III) complex (IOPS-iron) was synthesized and characterized. The IOPS-iron complex was found to have good digestive availability and good antioxidant activities on DPPH radicals and lipid peroxidation (Wang et al., 2015). A water-soluble polysaccharide from marine green algae *Ulva Pertusa* was isolated and polysaccharide-iron (III) complex was synthesized which was proved to enhance the activities of mice macrophages and promote the hematopoietic capacity of mice (Gao et al., 2019). The polysaccharide-iron complex has high digestibility and anti-radiation activity with low toxicity (Shi et al., 2013) and can retain the activities of polysaccharides and metal ions and enhance their activities (Chen and Huang, 2020). Meanwhile, the polysaccharide-iron (III) can lower blood sugar and promote blood circulation (Cui et al., 2017). Compared with inorganic iron compounds such as ferrous sulfate, polysaccharide iron complex does not cause gastrointestinal discomfort because the iron ions are bound rather than free (Dias et al., 2011).

Flammulina velutipes as a traditional fungus that is widely consumed in China belongs to the genus *Agaricaceae Tricholomaceae*. Meanwhile, *F. velutipes* is rich in nutrients such as protein, carbohydrates, vitamins and eight essential amino acids (Jing et al., 2014). Polysaccharide *from F. velutipes* (FVP) is a physiologically active substance extracted by water, ultrasonic and enzymatic method, etc. (Wang & Zhang, 2021). FVP had the functions of immune regulation, anti-tumor, liver protection, anti-oxidation, memory improvement, anti-fatigue and so on (Zhao et al., 2019; Song et al., 2021; Fu et al., 2019). *F. velutipes* scraps is the waste after picking *F. velutipes*. However, there are few reports on polysaccharides from *F. velutipes* scraps, especially their chelation with metal ions.

In this paper, a novel polysaccharide FVSP was extracted and purified from *F. velutipes* scraps. FVSP-iron (III) complex was synthesized by chelating with iron (III). The optimal preparation process of FVSP-iron (III) was investigated by response surface methodology. FVSP-iron (III) was characterized by UV–vis, FI-IR, thermogravimetric analysis and X-ray diffraction. In addition, the antioxidant activity in vitro of FVSP-iron (III) was also evaluated compared with FVSP.

2. Materials and methods

2.1. Materials

F. velutipes scraps was provided by an edible fungus breeding farm in Wuxi, Jiangsu province, China. 1,1-diphenyl-2-picrylhydrazyl (DPPH) was purchased from Sigma Aldrich (Sigma, St Louis, MO, USA). 2-Amino-2-hydroxymethyl-1,3-propanediol (Tris) was purchased from Acmec (Shanghai, China). Sodium citrate, absolute ethanol, hydrogen peroxide, *n*-butanol, trichloromethane, ferric chloride hexahydrate, ammonium ferrous sulfate, sodium acetate, salicylic acid, pyrogallol and other chemicals used in this paper were of analytical reagent grade.

2.2. Extraction, isolation and purification of FVSP

The fresh *F. velutipes* scraps was washed to remove impurities, dried and ground into powder. The dried powder was extracted with water at 75 °C for 160 min. The extract was centrifuged at 2266×g at 20 °C for 10 min.The supernatant was obtained and concentrated by vacuum evaporation in a rotary evaporator. The concentrated supernatant was precipitated

with 95 % ethanol and recovered by centrifugation at 11190 × g at 20 °C for 10 min. The precipitate was freeze-dried to obtain the crude polysaccharides. Then the crude polysaccharides were purified by anion-exchange chromatography on a DEAE-Sepharose CL-6B and size-exclusion chromatography on a Sephadex-G200 column. A novel fraction with higher antioxidant activity was collected and lyophilized, which was named FVSP.

2.3. Preparation of FVSP-iron (III)

FVSP-iron (III) was prepared according to the previous literature (Tang et al. 2013). FVSP (1 g), sodium citrate (0.5 g) and 20 mL distilled water were mixed. The mixed solution was heated and kept at 70 °C. Then the mixed solution was added to ferric chloride hexahydrate solution (2 mol/L) dropwise and stirred continuously. The pH was adjusted to 8.0–8.5 by sodium hydroxide solution (2 mol/L).

The addition of ferric chloride hexahydrate solution and sodium hydroxide solution was stopped when a reddish-brown insoluble precipitate appeared in the reaction solution. The reaction solution was kept at 70 °C for at least 1 h. Then the solution was centrifuged at 2266 × g for 10 min. The supernatant was precipitated with absolute ethanol. The pellet was centrifuged and freeze-dried to obtain FVSP-iron (III).

2.4. Determination of the chelation rate of FVSP-iron (III)

The chelation rate of FVSP-iron (III) was calculated based on the iron content with reference to the previous method (Tang et al. 2013). The iron content of FVSP-iron (III) was determined by phenanthroline colorimetry with ammonium ferrous sulfate standard solution. FVSP (20 mg) and FVSP-iron (III) (20 mg) were dissolved in 50 mL distilled water, respectively. Sample (10 mL) was mixed with 1 mL hydroxylamine hydrochloride (0.5 mol/L), 2.5 mL O-phenanthroline chromogenic (0.1 mol/L) and 5 mL sodium acetate buffer (1 mol/L, pH 4.5). The mixture was diluted to 50 mL with distilled water and shaken well. After 15 min, measurement of the absorbance of the solution at 510 nm was carried out. The iron content was calculated according to the calibration curve which was obtained by using ammonium ferrous sulfate standard solution ($Y = 0.0039X -0.0145$, $R^2 = 0.9904$). Chelation rate of FVSP-iron (III) was calculated based on the following formula.

Chelation rate$(\%) = (C_1 V_1 / m_1 - C_0 V_0 / m_0) \times 100$

where C_1 and C_0 were iron concentrations calculated from the standard curve of FVSP and FVSP-iron(III), respectively. V_1 and V_0 were dilution volume of 50 mL, m_1 and m_0 were 20 mg which was the quality of FVSP and FVSP-iron (III), respectively.

2.5. Single factor experiment of FVSP-iron (III) preparation

2.5.1. Effect of different reaction temperature on the chelation rate of FVSP-iron (III)

According to the method of preparation of FVSP-iron (III) as described above, FVSP (1 g) and sodium citrate (0.5 g) were added to the reaction system. The reaction system was kept at 50, 60, 70, 80 and 90 °C for 3 h, respectively. The chelation

rate of FVSP-iron (III) was determined to study the effect of reaction temperature on iron chelating rate of FVSP-iron (III).

2.5.2. Effect of different reaction time on the chelation rate of FVSP-iron (III)

FVSP (1 g) and sodium citrate (0.5 g) were added to the reaction system. The reaction system was kept at 70 °C for 1, 2, 3, 4, 5 and 6 h, respectively. The chelation rate of FVSP-iron (III) was determined to study the effect of reaction time on iron chelating rate of FVSP-iron (III).

2.5.3. Effect of the mass ratio of FVSP/sodium citrate on the chelation rate of FVSP-iron (III)

FVSP and sodium citrate were put into the reaction system at the mass ratio of 1:2, 1:1, 2:1, 3:1 and 4:1, respectively, and reacted at 70 °C for 3 h. The chelation rate of FVSP-iron (III) was determined to study the effect of mass ratio of FVSP/sodium citrate on iron chelating rate of FVSP-iron (III).

2.6. Experimental design of RSM

Experiments were designed using design expert software trial version 8.0 (Stat-Ease, Minneapolis). On the basis of single tests, a three-level three-factor Box–Behnken Design (BBD) was selected to evaluate the effect of three independent variables including reaction temperature (A), time (B), and the mass ratio of FVSP/sodium citrate (C). The independent variables were divided into three levels with $+1, 0, -1$, indicating high, medium and low values, respectively. The chelation rate of FVSP-iron (III) was set as the response.

2.7. Characterization of FVSP-iron (III)

2.7.1. Chemical composition analysis of FVSP-iron (III)

Protein content was determined by bicinchoninic acid assay (BCA) kit (Krieg, Dong, Schwamborn, & Knuechel, 2005). Briefly, the BCA protein assay kit was used to determine protein content based on the manufacturer's instructions. 25 μL FVSP-iron (III) solution (10 mg/mL) was added to the 96-well plate and mixed with 200 μL BCA working solution to each well and shaken for 30 s. Then the mixture was placed at 37 °C for 30 min and cooled to room temperature. The absorbance at 562 nm was measured on a microplate reader. The protein concentration was calculated and quantified according to the standard curve. Uronic acid content was determined by *meta*-hydroxy-diphenyl method (Filisetticozzi & Carpita, 1991) with some modification. 10 mg FVSP-iron (III) was mixed with deionized water to prepare a solution with uronic acid content of about 20–60 μg/mL. 1.0 mL sample solution and 6 mL sodium tetraborate-sulfuric acid solution were (0.012 mol/L) shaken and mixed. The mixture was heated at 100 °C for 5 min and then cooled to room temperature in an ice bath. The mixture was added into 0.1 mL m-hydroxybiphenyl reagent (0.15 %), shaken well and stand for 20 min. The absorbance at 520 nm was measured. Deionized water was used as a blank control. A standard curve was drawn with the content of galacturonic acid as the abscissa and OD_{520} as the ordinate. The uronic acid content was then calculated from a standard regression equation. Monosaccharide composition of FVSP-iron (III) was analyzed using the reported method (Sun et al., 2009). Briefly, 10 mL trifluoroacetic acid (2 mol/L) was used to hydrolyze FVSP-iron (III) (10 mg) at 105 °C for 6 h. Ethanol was used to precipitate the hydrolyzate. The hydrolyzate was freeze-dried and then mixed with 0.1 mL pyridine, hydroxylammonium (3 mg) and inositol (1 mg) at 90 °C for 30 min. After dissolution, the mixture was cooled to room temperature and then added into 0.1 mL acetic anhydride. The solution was incubated at 90 °C for 30 min. Gas chromatography was used to analyze monosaccharide composition. The operating conditions were as follows: flow rate of H_2, air and N_2 was 1.5 mL/min, 200 mL/min and 1.5 mL/min, respectively. Temperature of detector and column was 250 °C and 212 °C, respectively. The sulfate of FVSP and FVSP-iron (III) was determined according to the barium chloride-gelatin method (Cheng et al., 2019). FVSP (10 mg) and FVSP-iron (III) (10 mg) were added into 5 mL hydrochloric acid (1 mol/L) respectively for hydrolysis. The hydrolyzate was filtered to discard the residue. 0.5 mL hydrolyzate was mixed with 2.5 mL hydrochloric acid (1 mol/L) and 3 mL barium chloride-gelatin solution (0.5 %) for 15 min. The absorbance of reaction solution at 360 nm was determined. Fe (III) content was analyzed according to the previous method (Wang, Chen, Wang, & Xing, 2015). FVSP-iron (III) (5 mg) was added into 10 mL distilled water. FVSP-iron (III) solution (1 mL) was added into 5 mL water. The pH of the mixture was adjusted to 5.0 with hydrochloric acid (4.8 mol/L). Then the mixture was added into 0.1 mL ascorbic acid (0.1 g/mL), 2.0 mL sodium acetate trihydrate buffer solution (pH 4.5), and 1.0 mL 1,10-phenanthroline (1.0 g/L). The mixture was left to stand for 20 min. UV–vis detection was carried out at 510 nm. A calibration curve was obtained using a standard solution of ferrous ammonium sulfate in distilled water to calculate the Fe (III) content of FVSP-iron (III).

2.7.2. Molecular weight analysis

The average molecular weight of FVSP and FVSP-iron (III) was determined by high performance gel permeation chromatography. The measurement conditions were as follows. Mobile phase was 0.1 mol/L sodium nitrate solution. Flow rate was 0.9 mL/min and column temperature was 45 °C.

2.7.3. Ultraviolet–visible spectra

UV–vis spectra of FVSP and FVSP-iron (III) was recorded using a dual-beam scanning UV–vis spectrophotometer (UV6100, Shanghai Meipuda Instrument Co., ltd. Shanghai, China). The wavelength range was 200–600 nm.

2.7.4. FT-IR analysis

FSVP (1 mg) and FSVP- iron (III) powder (1 mg) were dried and mixed with potassium bromide separately and then pressed into pellets. FT-IR analysis was performed on an FT-IR spectrophotometer (Nicolet 6700, Thermo Scientific, USA) in the range of 400–4000 cm^{-1}.

2.7.5. X-ray diffraction analysis

X-ray diffraction of FVSP and FVSP-iron (III) were analyzed at the range of 10-80° at a scan rate of 0.5°/min using CuKα radiation on an X-ray diffractometer (SCX mini, Rigaku Inc., Tokyo, Japan).

2.7.6. Thermogravimetric analysis

FVSP (1 mg) and FVSP-iron (III) (1 mg) were put into the sample dish, respectively. Then thermogravimetric analysis (TGA) of FVSP and FVSP-iron (III) was performed from 40 to 800 °C at a heating rate of 10 °C/min using a thermo gravimetric analyzer (WRT-11, Beijing Beiguang Hongyuan Instrument Co., ltd., Beijing, China).

2.7.7. Surface morphology analysis

Surface morphology of FVSP and FVSP-iron (III) were analyzed using scanning electron microscope (SEM) (Ultra Plus, Zeiss, Germany). The FVSP and FVSP-iron (III) powders were placed on the sample stage and sprayed with gold powder. Each sample was observed with 2000 fold magnification at 20 kV voltage.

2.8. Antioxidant activities of FVSP-iron (III)

2.8.1. Hydroxyl radical scavenging activity (Hydroxyl RSA)

The hydroxyl radical scavenging activity of FVSP and FVSP-iron (III) was determined according to the reported method (Yu et al., 2019). FVSP and FVSP-iron (III) aqueous solution (1 mL) (0.2, 0.4, 0.6, 0.8 and 1.0 mg/mL) were mixed with 1 mL salicylic acid–ethanol (9 mmol/L), 1 mL ferrous sulfate (9 mmol/L) and 1 mL hydrogen peroxide (8.8 mmol/L), respectively. The mixture was incubated at 37 °C for 30 min and then the absorbance at 510 nm was measured. Distilled water was used as control. All experiments were carried out in triplicate and averaged. The hydroxyl RSA was calculated using the following equation.

$$Hydroxyl\ RSA(\%) = [1 - (A_i - A_j)/A_0] \times 100$$

where A_i was the absorbance of reaction mixture. A_j was the absorbance of reaction mixture without salicylic acid–ethanol replacing with distilled water. A_0 was the absorbance of reaction mixture without sample replacing with distilled water.

2.8.2. DPPH free radical scavenging activity (DPPH RSA)

The DPPH radical scavenging activity was determined according to the reported method (Li & Shah, 2013). FVSP and FVSP-iron (III) aqueous solution (2 mL) (0.2, 0.4, 0.6, 0.8 and 1.0 mg/mL) was mixed with 2 mL DPPH ethanol solution (25 mg/L). The mixture was kept in the dark for 30 min at room temperature and the absorbance was measured at 517 nm. The DPPH RSA was calculated using the following equation.

$$DPPH\ RSA(\%) = [A_0 - (A - A_b)]/A_0 \times 100$$

where A_0 was the absorbance of DPPH solution without sample replacing with distilled water. A was the absorbance of the test sample mixed with DPPH solution and A_b was the absorbance of the sample without DPPH solution replacing with distilled water.

2.8.3. Superoxide anion radical scavenging activity (Superoxide anion RSA)

The superoxide anion radical scavenging assay was measured by pyrogallol autoxidation method (Li & Shah, 2013). FVSP and FVSP-iron (III) aqueous solution (1 mL) (0.2, 0.4, 0.6, 0.8 and 1.0 mg/mL) was mixed with 4.5 mL Tris-HCl (50 mmol/L, pH 8.2). The mixture was incubated at 25 °C for 20 min. Then 0.3 mL pyrogallol (3 mmol/L, dissolved in 10 mmol/L hydrochloric acid) was added to the mixture and shaken rapidly. The absorbance was measured at 325 nm every 30 s. Superoxide anion RSA was calculated using the following equation.

$$Superoxide\ anion\ RSA(\%) = (1 - A/A_0) \times 100$$

where A_0 was the absorbance of mixture solution without sample replacing with distilled water. A was the absorbance of the test sample mixed with reaction solution.

2.9. Statistical analysis

Data analysis was performed using a Design Expert® software. Analysis of Variance (ANOVA) program was used to analyze variance and significant differences. Differences with $p < 0.05$ were considered statistically significant.

3. Results and discussion

3.1. Effect of different reaction temperature on chelation rate of FVSP-iron (III)

Effect of temperature on chelation rate was shown in Fig. 1 (A). When temperature rose from 40 to 50 °C, the chelation rate increased rapidly and up to a peak value of 4.41 ± 0.08 %. When temperature exceeded 50 °C, the chelation rate declined. The results showed that proper temperature promoted iron chelation into FVSP. However, too high temperature might cause the dissociation of FVSP-iron (III). Therefore, 50 °C was the suitable reaction temperature.

Effect of reaction time on chelation rate of FVSP-iron (III) was shown in Fig. 1(B). From 0 to 5 h, the chelation rate of FVSP-iron (III) increased slowly and up to a highest value of 4.23 ± 0.14 %. After that, the chelation rate decreased, which might be caused by the dissociation of some FVSP-iron (III).

Sodium citrate was a catalyst for iron chelation of polysaccharides. In the case of excessive iron in the reaction system, the mass ratio of polysaccharides to sodium citrate was a key parameter. Fig. 1(C) illustrated the effect of the mass ratio of FVSP/sodium citrate on chelation rate. As shown in Fig. 1 (C), excessive FVSP or sodium citrate would reduce the chelation rate of FVSP-iron (III). The most appropriate mass ratio of FVSP/sodium citrate was 3:1. Under this optimal ratio, the chelation rate reached 4.12 ± 0.12 %.

3.2. Box-Behnken design and analysis

Based on single factor experimental results, factors and levels designed for RSM were shown in Table1.The preparation process of FVSP-iron (III) was further optimized by RSM using Box-Behnken design (BBD). There were 17 experiments for optimizing the three individual parameters in current BBD. Each experiment was repeated three times. Results for response surface analysis were shown in Table 2. According to the multiple regression analysis, the response variable and the test variables were related by the following second-order polynomial equation.
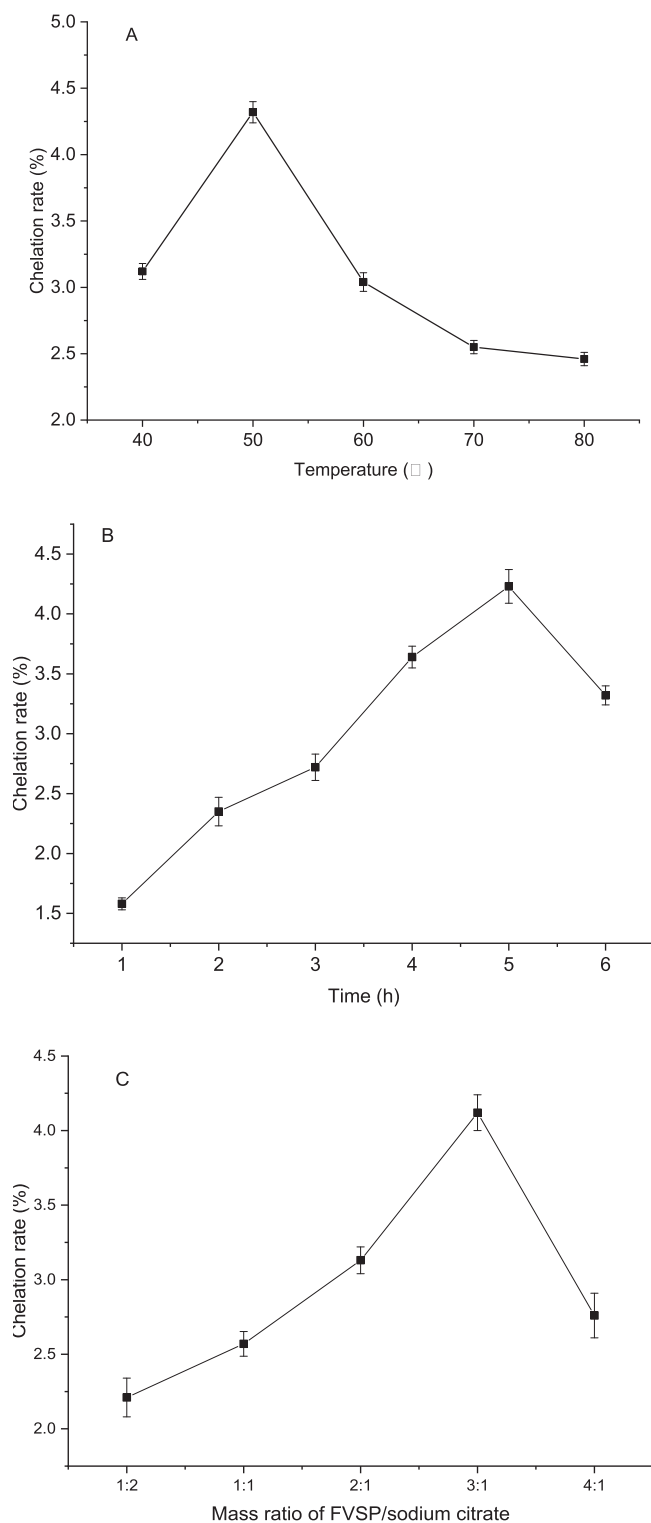
Fig. 1   Effect of reaction temperature (A), time (B) and mass ratio of FVSP/sodium citrate (C) on the chelation rate of FVSP-iron (III). Values were presented as means ± SD (*n* = 3).

$Y = 4.43 + 0.23A - 0.088B + 0.14C - 0.012AB - 0.093AC - 0.052BC - 0.55A^2 - 0.33B^2 - 0.038C^2$. The analysis of the experimental results of the BBD was summarized in Table 3. The F-value of the model was 31.20155 and p-value was lower than 0.0001,

which indicated that the model was reasonable. Lack of fit was not significant (F = 2.12246, p = 0.2401), which implied that other factors had little interference to the chelation rate and indicated that the model equation was appropriate to predict the chelation efficient of FVSP-iron (III) under any combination of values. According to this model, *A*, *B*, *C*, A^2 and B^2 are significant model terms (p < 0.05). The correlation coefficient (R^2 = 0.9757) indicated that the total variation of 97.57 % was attributed to the independent variables. The adjusted correlation coefficient (R^2_{adj} = 0.9444) and the CV value (C.V. % = 2.37 %) showed that the model had high fitting degree and high precision. These results showed that the regression equation could exhibit the true relationship between the response value and the various factors. The regression equation could be used to choose the best chelation technology conditions.

3.3. Optimization of chelation process of FVSP-iron (III)

The 3D response surface was presented in Fig. 2(A-C) to determine optimal levels of the test variables for the chelation of FVSP-iron (III).The effect of reaction temperature, reaction time and their interactions on chelation rate of FVSP-iron (III) were shown in Fig. 2(A). The effect surface of temperature was steeper than that of reaction time, which implied that the effect of temperature on chelation rate was more significant. The effect surface of temperature was steeper than that of the mass ratio of FVSP/sodium citrate, which indicated that the effect of temperature on chelation rate was more significant (Fig. 2(B)). Fig. 2(C) displayed the effect of reaction time, the mass ratio of FVSP/sodium citrate and their interactions on chelation rate of FVSP-iron (III), which indicated that the effect of mass ratio of FVSP/sodium citrate on chelation rate was more significant.

On basis of regression model analysis, the optimal values of the variables affecting the chelation rate of FVSP-iron (III) were reaction temperature of 50.41 °C, reaction time of 4.70 h and the mass ratio of FVSP/sodium citrate of 2.04:1. Under this conditions, the predicted chelation rate was 4.59 %. In view of the operating convenience, the optimal parameters were determined to be reaction temperature of 50 °C, reaction time of 4.70 h and the mass ratio of FVSP/sodium citrate of 2:1. Under this conditions, the chelation rate of FVSP-iron (III) was 4.55 ± 0.12 %. The results indicated that the model was satisfactory for the preparation process of FVSP-iron (III).

Our findings differed from those previously reported. *Grifola frondosa* polysaccharide-iron (III) complex (GFP-iron) was synthesized and the iron content of GFP-iron (III) complex reached 24.15 % (Xu et al., 2018). *Astragalus membranaceus* polysaccharide-iron (III) complex (APS-iron) was synthesized with the highest iron content (19.32 %) (Lu et al., 2016). There are many factors affecting the chelation rate of polysaccharides and iron (III), including temperature, time, and the addition ratio of sodium citrate to polysaccharides, etc. Different polysaccharides have different hydroxyl and carboxyl group contents due to their different structure. The hydroxyl and carboxyl groups in the polysaccharide molecule are electron-donating groups with strong nucleophilic ability and are easy to coordinate with metal ions. So the chelation of different polysaccharides and iron ions is also dif-

Table 1 Independent variables and levels of the experimental design.

Independent variable	levels		
	−1	0	1
A: reaction temperature (°C)	40	50	60
B: reaction time (h)	4.0	5.0	6.0
C: the mass ratio of FVSP/sodium citrate	2:1	3:1	4:1

Table 2 Experimental design and results for response surface analysis.

Runs	A	B	C	Chelation rate (%)
1	1	1	0	3.65
2	0	0	0	4.52
3	1	−1	0	3.87
4	−1	0	1	3.89
5	0	0	0	4.38
6	0	1	−1	3.96
7	1	0	1	4.21
8	0	0	0	4.49
9	0	1	1	4.01
10	0	−1	1	4.27
11	−1	1	0	3.26
12	−1	−1	0	3.43
13	−1	0	−1	3.29
14	0	0	0	4.42
15	1	0	−1	3.98
16	0	−1	−1	4.01
17	0	0	0	4.33

Table 3 Analysis of variance for the fitted quadratic polynomial model.

Source of variation	Sum of squares	df	Mean square	F-value	p-value
Model	2.524517	9	0.280502	31.20155	< 0.0001**
A	0.4232	1	0.4232	47.07453	0.0002**
B	0.06125	1	0.06125	6.813126	0.0349*
C	0.16245	1	0.16245	18.07008	0.0038**
AB	0.000625	1	0.000625	0.069522	0.7996
AC	0.034225	1	0.034225	3.807008	0.0920
BC	0.011025	1	0.011025	1.226363	0.3047
A^2	1.263284	1	1.263284	140.5211	< 0.0001**
B^2	0.452295	1	0.452295	50.3109	0.0002**
C^2	0.006	1	0.006	0.667438	0.4409
Residual	0.06293	7	0.00899		
Lake of fit	0.03865	3	0.012883	2.12246	0.2401
Pure error	0.02428	4	0.00607		
Total	2.587447	16			
R^2	0.9757				
R^2_{adj}	0.9444				
C.V.%	2.37				

Notes: * indicated significant difference ($p < 0.05$); ** indicated extremely significant difference ($p < 0.01$).

ferent, resulting in different chelation rate or iron content of polysaccharide-iron complex.

3.4. Chemical composition analysis

Chemical compositions of FVSP and FVSP-iron (III) were presented in Table4. Compared with FVSP, due to the addition of iron (III) to FVSP-iron (III), the content of protein, uronic acid and sulfate groups in FVSP-iron (III) decreased to a certain extent, respectively. The uronic acid and sulfate groups in the polysaccharide have a strong affinity for cations and the greatest binding force to cations (Li et al., 2019).The result suggested that iron ions reacted with uronic acid and sulfuric acid groups to synthesize complex. The iron content of FVSP-iron (III) was 6.27 %. Fe (III) is probably bound to sulfate and carboxyl groups (Cheng et al., 2019). Compared with AGSP, the contents of protein, uronic acid, and sulfate group of AGSP-Fe(III) decreased 0.36 %, 5.89 %, and 2.09 %, respectively, because of the addition of Fe(III) in the chemical composition of AGSP-Fe(III) complex (Wang et al.,2020).The monosaccharides in FVSP were glucose, galactose, mannose and xylose with a molar ratio of 56.2:18.2:10.9:14.7. The monosaccharides in FVSP-Iron (III) were glucose, galactose, mannose and xylose in a molar ratio of 65.1:20.5:5.2:9.2. Change in monosaccharides molar ratio between FVSP and FVSP-Fe (III) suggested that iron ions interacted with residues of the sugar chain. Due to the different configuration of the C-2 hydroxyl group, the binding constant of mannose to metal ions is higher than that of other monosaccharides such as glucose and galactose (Bera and Patra, 2011).

3.5. Molecular weight

The average molecular weight of FVSP and FVSP-iron (III) was determined to be 36.68 kDa and 36.25 kDa, respectively.

The decrease in molecular weight of FVSP-iron (III) may be due to the loss of the protective polysaccharide sheath outside the complex during dialysis (Wang et al., 2008).

3.6. UV–vis analysis

The UV–vis spectra of FVSP and FVSP-iron (III) was presented in Fig. 3A. No significant absorption near 260 or 280 nm in FVSP and FVSP-iron (III) was observed, which indicated the content of proteins and nucleic acids was low. The reason for the significant increase in the absorption of FVSP-iron(III) in the range of 250 to 350 nm in comparison with FVSP may be that the UV–vis spectrum in the 250–350 nm region is related to the oxo → metal charge transfer transition, which may lead to Fe-O bond formation (Geetha et al., 1995). $OD_{310\ nm}$ usually reflects the number of Fe-O bonds (Wu et al., 2013). FVSP-iron (III) had a higher $OD_{310\ nm}$ compared with FVSP, which indicated that Fe-O bonds in FVSP-iron (III) were successfully formed.

3.7. FT-IR analysis

The FT-IR spectra of FVSP and FVSP-iron (III) was presented in Fig. 3B. FVSP and FVSP-iron (III) had characteristic absorption peaks of polysaccharides. The absorption peak around 3400 cm^{-1} and 2900 cm^{-1} was attributed to the stretching vibration of hydroxyl groups and the stretching vibration of C—H, respectively (Dong et al., 2018).

The stronger absorption peak of FVSP-iron (III) around 1700 cm^{-1} was attributed to the stretching vibrations of C=O in carboxyl group (Chi et al., 2018). The absorption peak of FVSP-iron (III) around 1400 cm^{-1} was assigned to the bending vibration of C–OH (Li et al., 2018). Characteristic absorption peak around 680 cm^{-1} in FVSP-iron (III) was unique to β-FeOOH, which indicated that aggregated β-
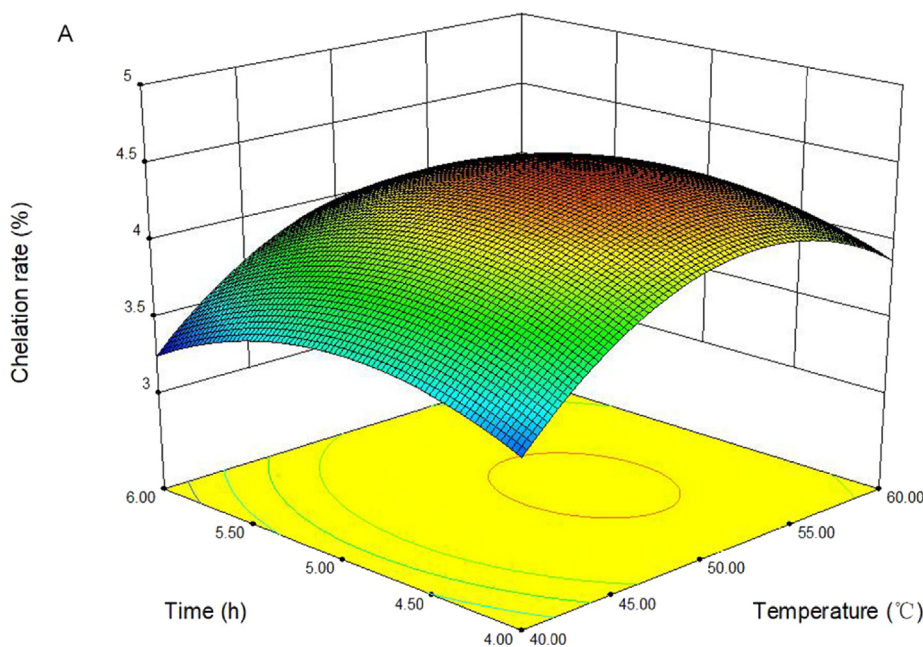
Fig. 2 Response surface plots showing the effect of reaction temperature, time, and mass ratio of FVSP/sodium citrate on the chelation rate of FVSP-iron (III).

B

C
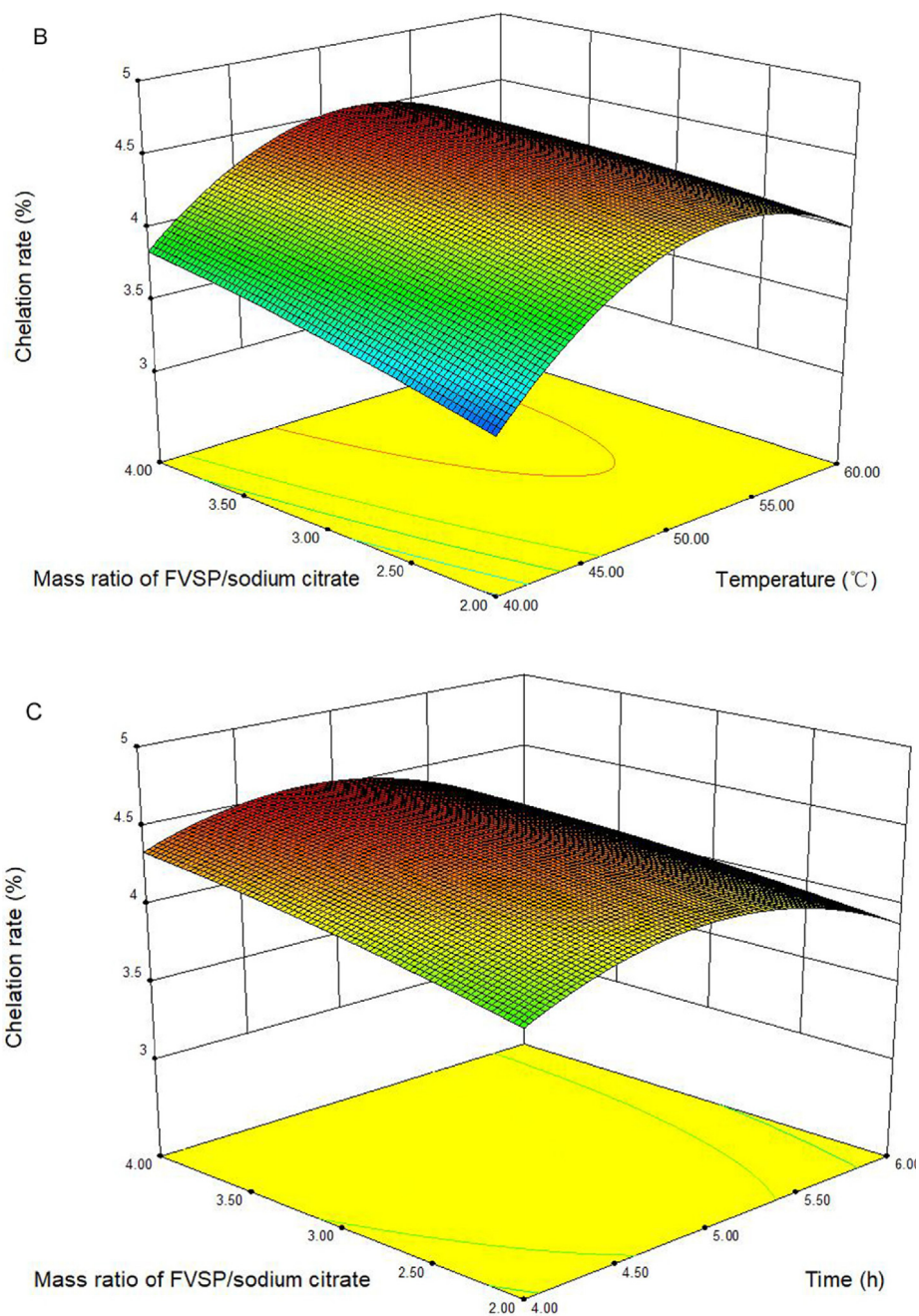
Fig. 2 (*continued*)

Table 4 Chemical compositions of FVSP and FVSP-iron (III).

Sample	Protein (%)	Uronic acid (%)	Sulfate (%)	Fe (%)	Monosaccharide (%)			
					Glucose	galactose	mannose	xylose
FVSP	3.36 ± 0.27	18.16 ± 1.19	8.79 ± 0.46	0	56.2	18.2	10.9	14.7
FVSP-iron (III)	3.02 ± 0.31	12.23 ± 0.56	6.27 ± 0.39	6.27 ± 0.39	65.1	20.5	5.2	9.2
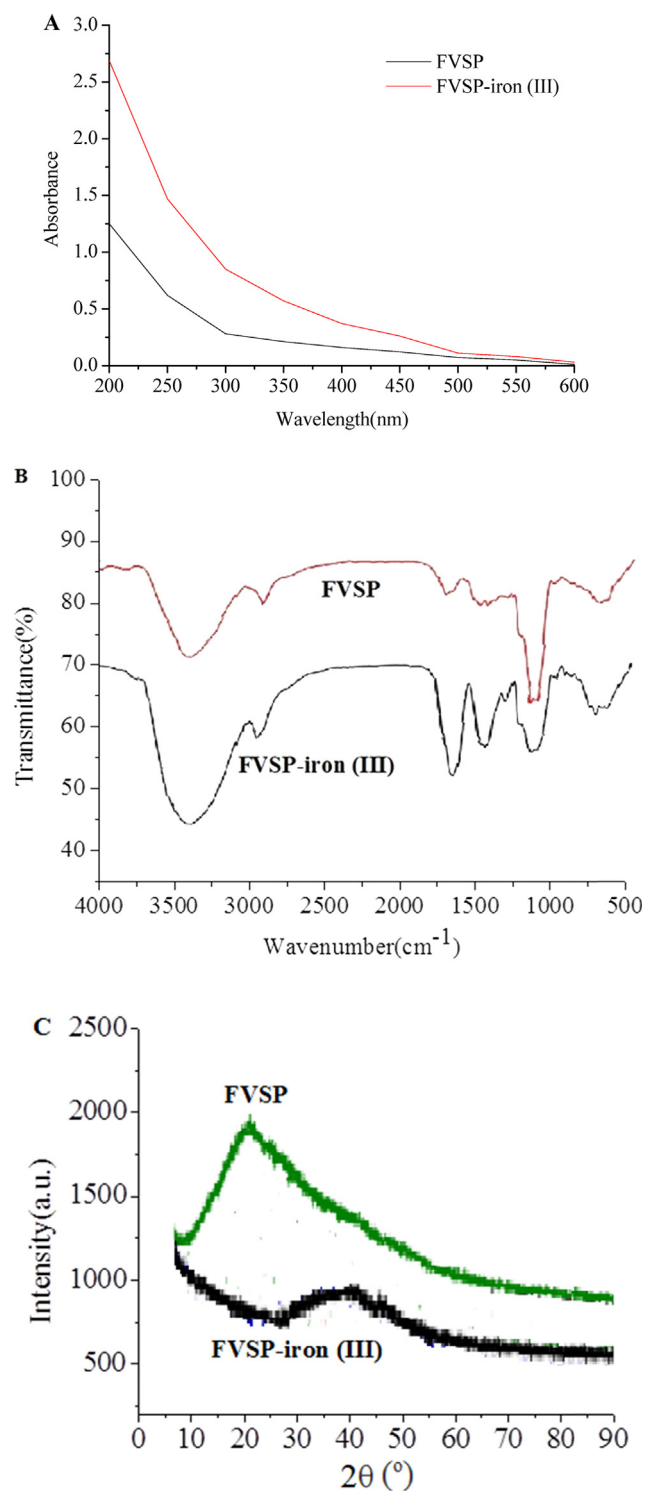
Fig. 4 Thermogravimetric curve of FVSP and FVSP-iron (III).

tinct characteristic peak ($2\theta = 20°$) of FVSP indicated "type II" crystals existed in FVSP. After the chelation of iron (III) and FVSP, iron (III) was introduced, thereby weakening the hydrogen bonding interaction (Lazaridis et al., 2007), Therefore, the peak ($2\theta = 20°$) disappeared on the X-ray diffraction spectrum of FVSP-iron (III). The diffraction peak ($2\theta = 40°$) on the X-ray diffraction spectrum indicated that the FVSP-iron (III) contained iron (III).

3.9. Thermogravimetric analysis

The thermogravimetric curve of FVSP and FVSP-iron (III) was shown in Fig. 4. The weight of FVSP-iron (III) did not decrease in the range of 200 °C.The weight of FVSP began to decrease beyond 150 °C because of the loss of physically bound water. The weight loss of FVSP and FVSP-iron (III) decreased rapidly because of the loss of chemically bound water when the temperature was between 200 and 600 °C. When the temperature exceeded 600 °C, the reduction in weight loss was relatively small. However, the weight loss of FVSP-iron (III) was slightly lower than that of FVSP within the heating temperature range, which indicated that FVSP-iron (III) had better thermal stability than FVSP.

3.10. Surface morphology of FVSP and FVSP-iron (III)

Surface morphology of FVSP and FVSP-iron (III) was presented in Fig. 5. As shown in Fig. 5(A), the surface of FVSP had less holes and the surface of FVSP-iron (III) had more holes. The surface of polysaccharides and polysaccharides-iron (III) differs because of the cooperation of Fe (III) and polysaccharides (Cheng et al., 2019). The center of polysaccharide iron complex is usually -FeOOH surrounded by polysaccharide (Zhang et al., 2017). The results suggested that the incorporation of Fe (III) into FVSP via Fe-O may alter the surface morphology of FVSP.

3.11. Antioxidant activities of FVSP and FVSP-iron (III)

Hydroxyl free radicals can react with most biomacromolecules to cause tissue damage (Teng et al., 2021). The scavenging

Fig. 3 Spectra of FVSP and FVSP-iron (III) (A: UV–vis; B: FT-IR; C: X-ray diffraction).

FeOOH iron cores existed in polysaccharide iron complexes (Coe, et al., 1995).

3.8. X-ray diffraction analysis

X-ray diffraction spectrum of FVSP and FVSP-iron (III) was presented in Fig. 3C. Compared with FVSP-iron (III), a dis-
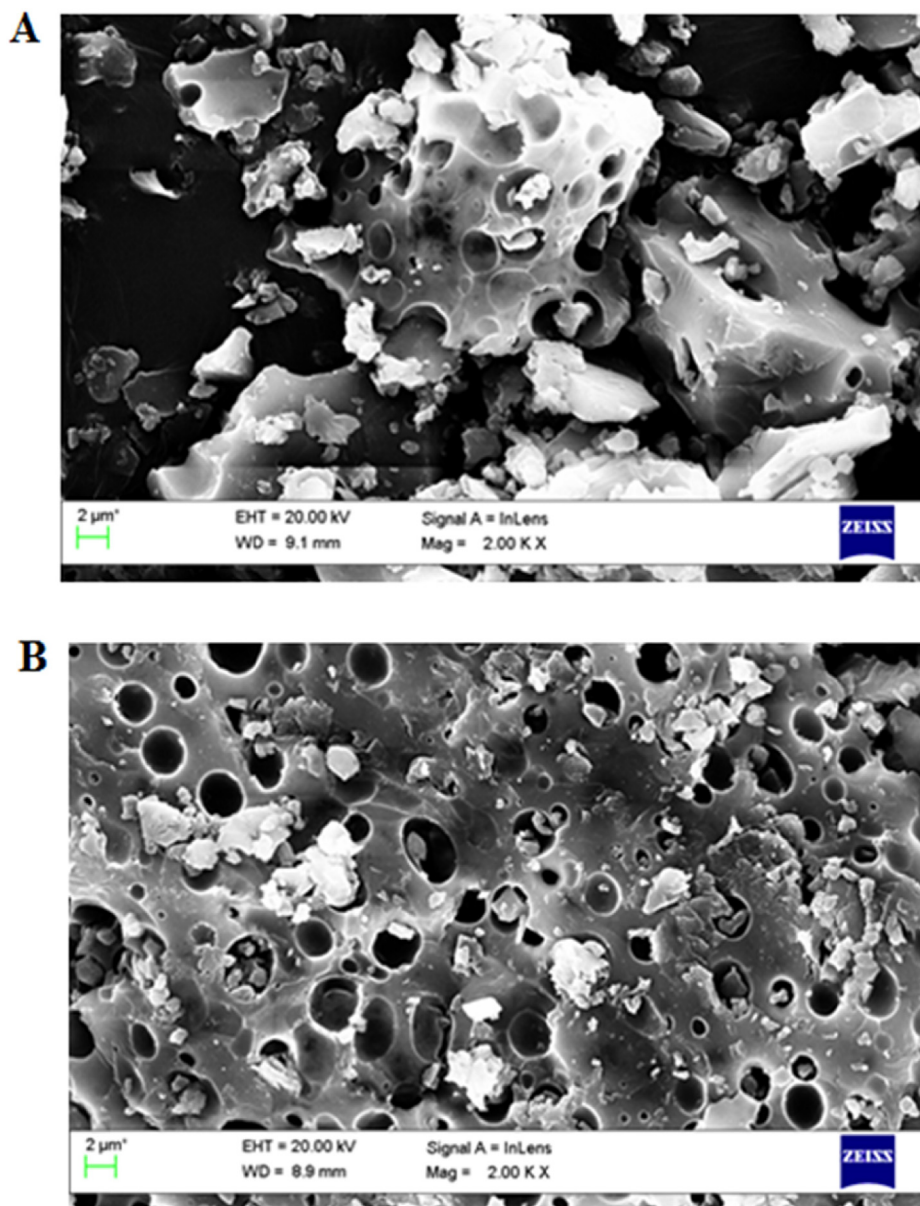
Fig. 5   Surface morphology of FVSP (A) and FVSP-iron (III) (B) using SEM.

activities of FVSP and FVSP-iron (III) on hydroxyl radicals were shown in Fig. 6 (A). The Hydroxyl RSA of FVSP and FVSP-iron (III) were both concentration-dependent. The scavenging activity of FVSP-iron (III) was significantly higher than that of FVSP within the tested concentrations. When the concentration was 1 mg/mL, the highest hydroxyl RSA of FVSP-iron (III) and FVSP was 52.12 ± 0.72 % and 40.42 ± 0.82 %, respectively.

DPPH is stable and can capture other free radicals to become stable molecules (Li et al., 2017). Therefore, DPPH is widely used to measure antioxidant activity. Fig. 6(B) indicated the scavenging effect of FVSP and FVSP-iron (III) on DPPH. The scavenging effect was also concentration-dependent. When the concentration was 1 mg/mL, the highest DPPH RSA of FVSP-iron (III) and FVSP was 56.87 ± 0.96 % and 42.43 ± 1.23 %, respectively.

Superoxide anion free radical can react with biological-macromolecules to induce tissue damage (Du et al., 2018). The scavenging effect of FVSP and FVSP-iron (III) on superoxide anion radical was shown in Fig. 6 (C). The superoxide anion RSA of FVSP was higher than that of FVSP-iron (III) within the sample concentration range in a concentration-dependent manner. When the c oncentration was 1 mg/mL, the highest superoxide anion RSA of FVSP-iron (III) was 81.53 ± 0.92 %, which was much higher than that (36.75 ± 1.23 %) of FVSP.

Lignin-rich lignin-carbohydrate complexes (LCC-A) from wheat straw possesses higher in vitro scavenging ability of reactive oxygen species and Carbohydrate-rich lignin-carbohydrate complexes (LCC-B) from wheat straw activates cellular antioxidant activities via the KEAP1-NRF2-ARE pathway (Zheng et al., 2021). Carbohydrate-rich Lignin-
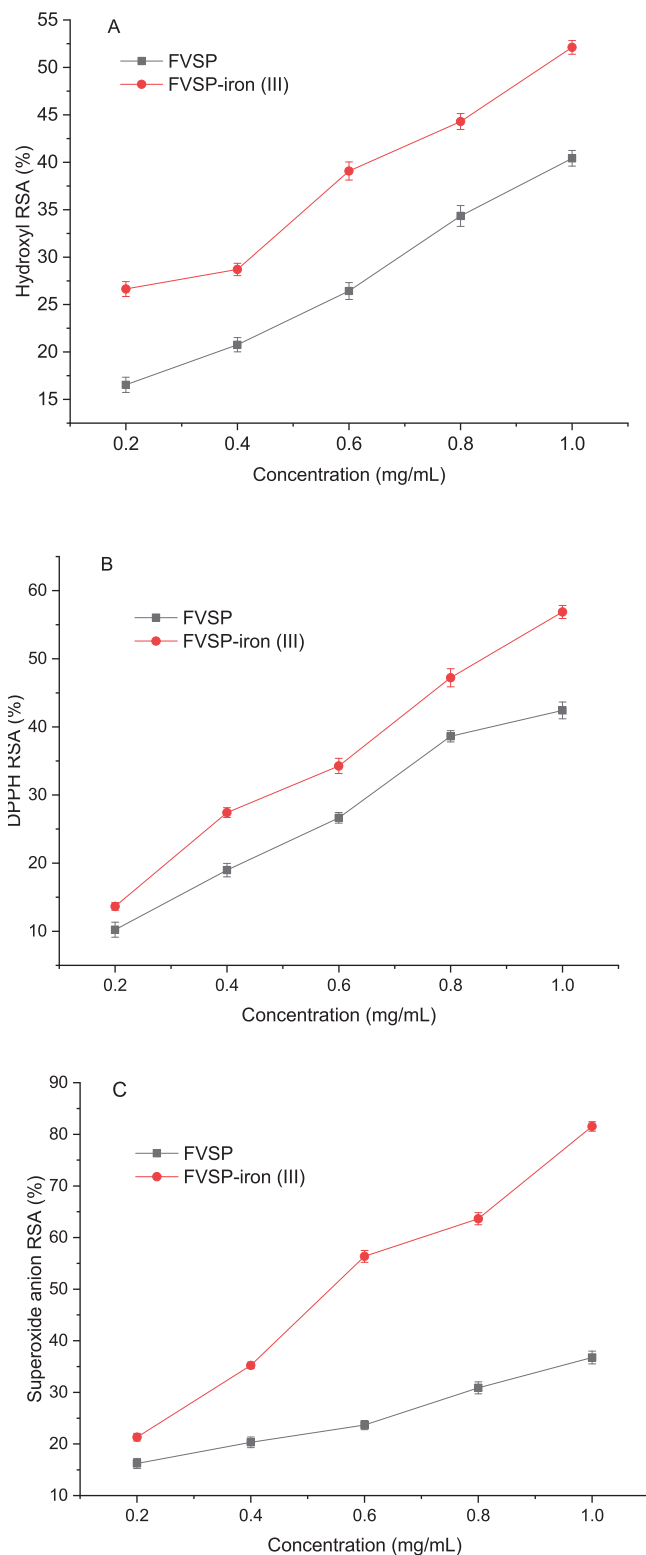
Fig. 6   The scavenging activities of FVSP and FVSP-iron (III) on hydroxyl radicals (A), DPPH radicals (B) and superoxide anion radicals(C). Values were presented as means ± SD ($n = 3$).

carbohydrate complexes from bamboo exhibited better antioxidant activities for scavenging the individual free radicals (Dong et al., 2020). Previous studies showed that iron-

chelating polysaccharides from different sources exhibit different antioxidant activities. Lu et al. found that a *Astragalus membranaceus* polysaccharide-iron(III) complex (APS-iron (III)) showed higher scavenging effect on DPPH free radical than that of *A. membranaceus* polysaccharide (APS), while the scavenging effect on hydroxyl free radical and ABTS of APS-iron(III) was lower than that of APS (Lu et al.,2016). Yu et al. investigated the antioxidant activities of polysaccharide-iron (III) chelates from the cocultured *Lepista sordida* and *Pholiota nameko*. The polysaccharide-iron (III) exhibited higher scavenging activity on hydroxyl free radical and superoxide anion free radical and lower scavenging activity on DPPH free radical (Yu, Jiang, & Li, (2020). Polysaccharide-iron (III) (CPS-iron) was extracted from *Cordyceps militaris* mycelia by adding ferrous sulfate solution to the mycelia. The CPS-iron had higher scavenging effect on DPPH free radical, but had few effect on hydroxyl free radical and superoxide anion free radical (Zhang et al., 2021). Our results showed that the scavenging effect of FVSP-iron (III) on hydroxyl radical, DPPH and superoxide anion radical were significantly increased after chelation, which indicated that FVSP-iron (III) enhanced the hydrogen donating ability and pairing with free radicals.

4. Conclusion

In this study, a novel polysaccharide FVSP was extracted and purified from *F. velutipes* scraps, which was chelated with iron to synthesize FVSP-iron (III). Through response surface analysis, the optimal preparation process of FVSP-iron (III) was obtained. Under the optimum conditions, the chelation rate of FVSP-iron (III) was 4.55 ± 0. 12 %. Hydroxyl and carboxyl groups in FVSP participated in the coordination reaction and the iron core of FVSP-Iron (III) was a polymerized β-FeOOH structure. FVSP-iron (III) exhibited better thermal stability and stronger antioxidant activities than FVSP. The results indicated that FVSP-iron (III) could be potentially used as a new food additive and multifunctional iron supplement in food industry. In the future, it is necessary to study the structure and antioxidant mechanism of FVSP-iron (III).

Declaration of Competing Interest

The authors declare that they have no known competing financial interests or personal relationships that could have appeared to influence the work reported in this paper.

References

Bera, M., Patra, A., 2011. Study of potential binding of biologically important sugars with a dinuclear cobalt (II) complex. Carbohyd. Res. 346 (6), 733–738.

Chen, X., Huang, G., 2020. Synthesis and antioxidant activities of garlic polysaccharide-Fe (III) complex. Int. J. Biol. Macromol. 145, 813–818.

Cheng, C., Huang, D.C., Zhao, L.Y., Cao, C.J., Chen, G.T., 2019. Preparation and in vitro absorption studies of a novel polysaccha-

ride-iron (III) complex from Flammulina velutipes. Int. J. Biol. Macromol. 132, 801–810.

Chi, Y.Z., Li, Y.P., Zhang, G.L., Gao, Y.Q., Ye, H., Gao, J., Wang, P., 2018. Effect of extraction techniques on properties of polysaccharides from *Enteromorpha prolifera* and their applicability in iron chelation. Carbohydr. Polym. 181, 616–623.

Coe, E.M., Bowen, L.H., Speer, J.A., Wang, Z., Sayers, D.E., Bereman, R.D., 1995. The characterization of a polysaccharide iron complex (Niferex). J. Inorg. Biochem. 58 (4), 269–278.

Cui, J., Li, Y., Yu, P., Zhan, Q., Wang, J., Chi, Y., Wang, P., 2017. A novel low molecular weight Enteromorpha polysaccharide-iron (III) complex and its effect on rats with iron deficiency anemia (IDA). Int. J. Biol. Macromol. 108, 412–418.

Danielson, B.G., 2004. Structure, chemistry, and pharmacokinetics of intravenous iron agents. J. Am. Soc. Nephrol. 15, 93–98.

Denic, S., Agarwal, M.M., 2007. Nutritional iron deficiency: an evolutionary perspective. Nutrition 23, 603–614.

Dias, A.M.G.C., Hussain, A., Marcos, A.S., Roque, A.C.A., 2011. A biotechnological perspective on the application of iron oxide magnetic colloids modified with polysaccharides. Biotechnol. Adv. 29, 142–155.

Dong, J.M., Li, H.M., Min, W.H., 2018. Preparation, characterization and bioactivities of Athelia rolfsii exopolysaccharide-zinc complex (AEPS-zinc). Int. J. Biol. Macromol. 113, 20–28.

Dong, H.L., Zheng, L.M., Yu, P.J., Jiang, Q., Wu, Y., Huang, C.X., Yin, B.S., 2020. Characterization and application of lignin-carbohydrate complexes from lignocellulosic materials as antioxidant for scavenging in vitro and in vivo reactive oxygen species. ACS Sustain. Chem. Eng. 8 (1), 256–266.

Du, X.J., Wang, X.D., Chen, Y., Tian, S.Y., Lu, S.F., 2018. Antioxidant activity and oxidative injury rehabilitation of chemically modified polysaccharide (TAPA1) from Tremella aurantialba. Macromol. Res. 26 (6), 479–483.

Filisetticozzi, T., Carpita, N.C., 1991. Measurement of uronic-acids without interference from neutral sugars. Anal. Biochem. 197, 157–162.

Fu, Y., Yuan, Q., Lin, S., Liu, W., Du, G., Zhao, L., Zhang, Q., Lin, D.R., Liu, Y.T., Qin, W., Li, D.Q., Wu, D.T., 2019. Physicochemical characteristics and biological activities of polysaccharides from the leaves of different loquat (*Eriobotrya japonica*) cultivars. Int. J. Biol. Macromol. 135, 274–281.

Gao, X., Qu, H., Gao, Z.L., Zeng, D.Y., Wang, J.P., Baranenko, D., Li, Y.Z., Lu, W.H., 2019. Protective effects of *Ulva pertusa* polysaccharide and polysaccharide iron (III) complex on cyclophosphamide induced immunosuppression in mice. Int. J. Biol. Macromol. 133, 911–919.

Geetha, K., Raghavan, M.S.S., Kulshreshtha, S.K., Sasikala, R., Rao, C.P., 1995. Transition-metal saccharide chemistry: synthesis, spectroscopy, electrochemistry and magnetic susceptibility studies of iron (III) complexes of mono-and disaccharides. Carbohyd. Res. 271, 163–175.

Huang, C.X., Tao, Y.H., Li, M., Zhang, W.Y., Fan, Y.M., Yong, Q., 2019. Synthesis and characterization of an antioxidative galactomannan–iron (III) complex from sesbania seed. Polymers. 11 (1), 28.

Jing, P., Zhao, S.J., Lu, M.M., Cai, Z., Pang, J., Song, L.H., 2014. Multiple-fingerprint analysis for investigating quality control of *Flammulina velutipes* fruiting body polysaccharides. J. Agr. Food Chem. 62, 12128–12133.

Krieg, R.C., Dong, Y., Schwamborn, K., Knuechel, R., 2005. Protein quantification and its tolerance for different interfering reagents using the BCA-method with regard to 2D SDS PAGE. J. Biochem. Bioph. Meth. 65, 13–19.

Lazaridis, N.K., Kyzas, G.Z., Vassiliou, A.A., Bikiaris, D.N., 2007. Chitosan derivatives as biosorbents for basic dyes. Langmuir 23 (14), 7634–7643.

Li, Y.Y., Chen, J.Y., Cao, L.L., Li, L., Wang, F., Liao, Z.P., Chen, J. J., Wu, S.H., Zhang, L.Y., 2018. Characterization of a novel polysaccharide isolated from Phyllanthus emblica L. and analysis of its antioxidant activities. J. Food Sci. Technol. 55 (7), 2758–2764.

Li, S., Shah, N.P., 2013. Effects of various heat treatments on phenolic profiles and antioxidant activities of *Pleurotus eryngii* extracts. J. Food Sci. 78, 1122–1129.

Li, C.Q., Sun, P., Yu, H.Y., Zhang, N., Wang, J., 2017. Scavenging ability of dendritic pamam bridged hindered phenolic antioxidants towards dpph· and roofree radicals. RSC Adv. 7, 1869–1876.

Li, Y., Wang, X., Jiang, Y., Wang, J., Wang, H.H., Yang, X., Wang, P., 2019. Structure characterization of low molecular weight sulfate Ulva polysaccharide and the effect of its derivative on iron deficiency anemia. Int. J. Biol. Macromol. 126, 747–754.

Lu, Q., Xu, L., Meng, Y.B., Liu, Y., Li, J., Zu, Y.G., Zhu, M.H., 2016. Preparation and characterization of a novel *Astragalus membranaceus* polysaccharide-iron (III) complex. Int. J. Biol. Macromol. 93, 208–216.

Sarah, C.C., Lorraine, G., Helen, E.H., Valerie, J.S., Harry, J.M., 2016. Pregnancy and maternal iron deficiency stimulate hepatic CRBPII expression in rats. J. Nutr. Biochem. 32, 55–63.

Shi, J., Cheng, C., Zhao, H., Jing, J., Gong, N., Lu, W., 2013. In vivo anti-radiation activities of the Ulva pertusa polysaccharides and polysaccharide-iron (III) complex. Int. J. Biol. Macromol. 60, 341–346.

Song, X., Fu, H., Chen, W., 2021. Effects of *Flammulina velutipes* polysaccharides on quality improvement of fermented milk and antihyperlipidemic on streptozotocin-induced mice. J. Funct. Foods. 87, 104834.

Sun, H.H., Mao, W.J., Chen, Y., Guo, S.D., Li, H.Y., Qi, X.H., Chen, Y.L., Xu, J., 2009. Isolation, chemical characteristics and antioxidant properties of the polysaccharides from marine fungus Penicillium sp. F23-2. Carbohydr. Polym. 78 (1), 117–124.

Tang, M.M., Wang, D.F., Hou, Y.F., Buchili, P., Sun, L.P., 2013. Preparation, characterization: bioavailability in vitro and in vivo of tea polysaccharides-iron complex. Eur. Food Res. Technol. 236, 341–350.

Teng, C., Qin, P.Y., Shi, Z.X., Zhang, W.Y., Yang, X.S., Yao, Y., Ren, G.X., 2021. Structural characterization and antioxidant activity of alkali-extracted polysaccharides from quinoa. Food Hydrocolloid. 113, 106392.

Wang, K.P., Chen, Z.X., Zhang, Y., Wang, P.P., Wang, J.H., Dai, L. Q., 2008. Molecular weight and proposed structure of the Angelica sinensis polysaccharide-iron complex. Chinese J. Chem. 26 (6), 1068–1074.

Wang, J., Chen, H., Wang, Y., Xing, L., 2015. Synthesis and characterization of a new Inonotus obliquus polysaccharide-iron (III) complex. Int. J. Biol. Macromol. 75, 210–217.

Wang, L.L., Wang, L.L., Su, C.Y., Wen, C.R., Gong, Y., You, Y., Zhao, J., Han, Y.H., Song, S., Xiao, H., 2020. Characterization and digestion features of a novel polysaccharide-Fe(III) complex as an iron supplement. Carbohydr. Polym. 249, 116812.

Wang, Y., Zhang, H., 2021. Advances in the extraction, purification, structural-property relationships and bioactive molecular mechanism of *Flammulina velutipes* polysaccharides: A review. Int. J. Biol. Macromol. 167, 528–538.

Wu, G.J., Li, Y.P., Hu, L., Chen, Z.Q., Hong, L.M., 2012. Synthesis of *Portulace oleracea* L. polysaccharide iron complex and its physical chemical properties. Food Sci. Tech. 37, 250–252.

Wu, H., Liu, Z., Dong, S., Zhao, Y., Huang, H., Zeng, M., 2013. Formation of ferric oxyhydroxide nanoparticles mediated by peptides in anchovy (Engraulis japonicus) muscle protein hydrolysate. J. Agr. Food Chem. 61 (1), 219–224.

Xu, L., Meng, Y.B., Liu, Y., Meng, Q.H., Zhang, Z.D., Li, J., Lu, Q., 2018. A novel iron supplements preparation from Grifola frondosa polysaccharide and assessment of antioxidant, lymphocyte proliferation and complement fixing activities. Int. J. Biol. Macromol. 108, 1148–1157.

Yu, M., Chen, M., Gui, J., Huang, S., Liu, Y., Shentu, H., He, J., Fang, Z., Wang, W., Zhang, Y., 2019. Preparation of *Chlorella vulgaris* polysaccharides and their antioxidant activity in vitro and in vivo. Int. J. Biol. Macromol. 137, 139–150.

Yu, S., Jiang, J., Li, W., 2020. Co-cultured *Lepista sordida* and *Pholiota nameko* polysaccharide-iron (III) chelates exhibit good antioxidant activity. RSC Adv. 10 (46), 27259–27265.

Zhang, Y., Ma, F., Zhu, J., Du, Z., Zhao, Y.Y., Liu, X., 2017. Characterization of a novel polysaccharide-Iron (III) complex and its anti-anemia and nonspecific immune regulating activities. Mini Rev. Med. Chem. 17 (17), 1677–1683.

Zhang, Z.S., Wang, X.M., Han, Z.P., Yin, L., Zhao, M.X., Yu, S.C., 2012. Physicochemical properties and inhibition effect on iron deficiency anemia of a novel polysaccharide-iron complex (LPPC). Bioorg. Med. Chem. Lett. 22, 489–492.

Zhang, X., Zhang, X., Gu, S., Pan, L., Sun, H., Gong, E., Zhu, Z., Wen, T., Daba, G.M., Elkhateeb, W.A., 2021. Structure analysis and antioxidant activity of polysaccharide-iron (III) from *Cordyceps militaris* mycelia. Int. J. Biol. Macromol. 178, 170–179.

Zhao, R., Hu, Q., Ma, G., Su, A., Xie, M., Li, X., Chen, G., Zhao, L., 2019. Effects of *Flammulina velutipes* polysaccharide on immune response and intestinal microbiota in mice. J. Funct. Foods. 56, 255–264.

Zheng, L.M., Yu, P.J., Zhang, Y.B., Wang, P., Yan, W.J., Guo, B.S., Huang, C.X., Qing Jiang, Q., 2021. Evaluating the bio-application of biomacromolecule of lignin-carbohydrate complexes (LCC) from wheat straw in bone metabolism via ROS scavenging. Int. J. Biol. Macromol. 176, 13–25.